The Astrophysical Journal Letters, 912:L32 (8pp), 2021 May 10 https://doi.org/10.3847/2041-8213/abf93d

SPLUS J210428.01−004934.2: An Ultra Metal-poor Star Identified from Narrowband Photometry*

Vinicius M. Placco[1], Ian U. Roederer[2,3], Young Sun Lee[4], Felipe Almeida-Fernandes[5], Fábio R. Herpich[5], Hélio D. Perottoni[5], William Schoenell[6], Tiago Ribeiro[7], and Antonio Kanaan[8]
[1] Community Science and Data Center/NSF's NOIRLab, 950 N. Cherry Avenue, Tucson, AZ 85719, USA; vinicius.placco@noirlab.edu
[2] Department of Astronomy, University of Michigan, Ann Arbor, MI 48109, USA
[3] JINA Center for the Evolution of the Elements, USA
[4] Department of Astronomy and Space Science, Chungnam National University, Daejeon 34134, Republic of Korea
[5] Departamento de Astronomia, Instituto de Astronomia, Geofísica e Ciências Atmosféricas da USP, Cidade Universitária, 05508-900, São Paulo, SP, Brazil
[6] GMTO Corporation 465 N. Halstead Street, Suite 250 Pasadena, CA 91107, USA
[7] Rubin Observatory Project Office, 950 N. Cherry Avenue, Tucson, AZ 85719, USA
[8] Departamento de Física, Universidade Federal de Santa Catarina, Florianópolis, SC 88040-900, Brazil
Received 2021 April 7; revised 2021 April 14; accepted 2021 April 15; published 2021 May 12

Abstract

We report on the discovery of SPLUS J210428.01−004934.2, an ultra metal-poor (UMP) star first identified from the narrowband photometry of the Southern Photometric Local Universe Survey (S-PLUS) Data Release 1, in the SDSS Stripe 82 region. Follow-up medium- and high-resolution spectroscopy (with Gemini South and Magellan-Clay, respectively) confirmed the effectiveness of the search for low-metallicity stars using the S-PLUS narrowband photometry. At [Fe/H] = −4.03, SPLUS J2104−0049 has the lowest *detected* carbon abundance, A(C) = +4.34, when compared to the 34 previously known UMP stars in the literature, which is an important constraint on its stellar progenitor and also on stellar evolution models at the lowest metallicities. Based on its chemical abundance pattern, we speculate that SPLUS J2104−0049 could be a bona fide second-generation star, formed from a gas cloud polluted by a single metal-free $\sim 30 M_{\odot}$ star. This discovery opens the possibility of finding additional UMP stars directly from narrowband photometric surveys, a potentially powerful method to help complete the inventory of such peculiar objects in our Galaxy.

Unified Astronomy Thesaurus concepts: High resolution spectroscopy (2096); Stellar atmospheres (1584); Narrow band photometry (1088); Chemical abundances (224); Metallicity (1031)

Supporting material: data behind figure, interactive figures

1. Introduction

Is there any observational evidence that the first generation of stars born in the universe (Population III) had an initial mass function (IMF) that allowed the formation of low-mass ($M \leqslant 1.0 M_{\odot}$) objects? Cosmological simulations indicate that the Population III IMF can extend to such low masses (Stacy et al. 2016). However, as of today, no metal-free stars have been found. Even the most chemically pristine star ever observed (SMSS J031300.36−670839.3; Keller et al. 2014) has lithium, carbon, oxygen, magnesium, and calcium detected in its atmosphere. Based on current theoretical work, molecular hydrogen cooling allows the formation of minihalos of $10^6 M_{\odot}$ as early as $z \approx 20$–30, which will fragment and form predominantly massive ($M > 10 M_{\odot}$) stars (Bromm 2013). Then, with the first chemical elements heavier than He introduced in the interstellar medium by the evolution of these massive objects, the formation of low-mass objects would be facilitated by additional cooling channels, such as dust and metal lines (in particular C II and O I; Dopcke et al. 2013). Alternatively, Schlaufman et al. (2018) found evidence implying that it is possible to have surviving (present-day) solar-mass stars that were secondaries around massive Population III stars ($10 \leqslant M/M_{\odot} \leqslant 100$), and were formed via disk fragmentation.

Ultra metal-poor (UMP; [Fe/H][9] <−4.0) stars (Beers & Christlieb 2005), while still members of the second generation, can provide an observational benchmark as to whether such low-mass metal-free stars exist. According to Hartwig et al. (2015), in order to rule out (at a 99% confidence level) the existence of a low-mass metal-free star, $\sim 2 \times 10^7$ halo stars should be observed and have their [Fe/H] determined. That translates into roughly several hundred observed UMP stars, although only 34[10] have been found to date (Suda et al. 2008; Abohalima & Frebel 2018).

One technique to select suitable UMP candidates for spectroscopic follow-up is through photometric metallicities. The first effort of estimating the metallicity from the Sloan Digital Sky Survey (SDSS; York et al. 2000) $u - g$ and $g - r$ colors was published by Ivezić et al. (2008). The authors were able to determine [Fe/H] for over 2 million F/G stars in the Milky Way with uncertainties of 0.2 dex or better for $-2.0 \leqslant$ [Fe/H] $\leqslant -0.5$. However, due to the intrinsic

* Based on observations gathered with the 6.5 m Magellan Telescopes located at Las Campanas Observatory, Chile. Based on observations obtained at the international Gemini Observatory, a program of NSF's NOIRLab, which is managed by the Association of Universities for Research in Astronomy (AURA) under a cooperative agreement with the National Science Foundation on behalf of the Gemini Observatory partnership: the National Science Foundation (United States), National Research Council (Canada), Agencia Nacional de Investigación y Desarrollo (Chile), Ministerio de Ciencia, Tecnología e Innovación (Argentina), Ministério da Ciência, Tecnologia, Inovações e Comunicações (Brazil), and Korea Astronomy and Space Science Institute (Republic of Korea).

[9] [A/B] = $\log(N_X/N_Y)_{\star} - \log(N_X/N_Y)_{\odot}$, where N is the number density of elements X and Y in the star ($\star$) and the Sun ($\odot$).
[10] High-resolution ($R \geqslant 20{,}000$) spectroscopy is required to derive [Fe/H] and classify a star as a UMP.

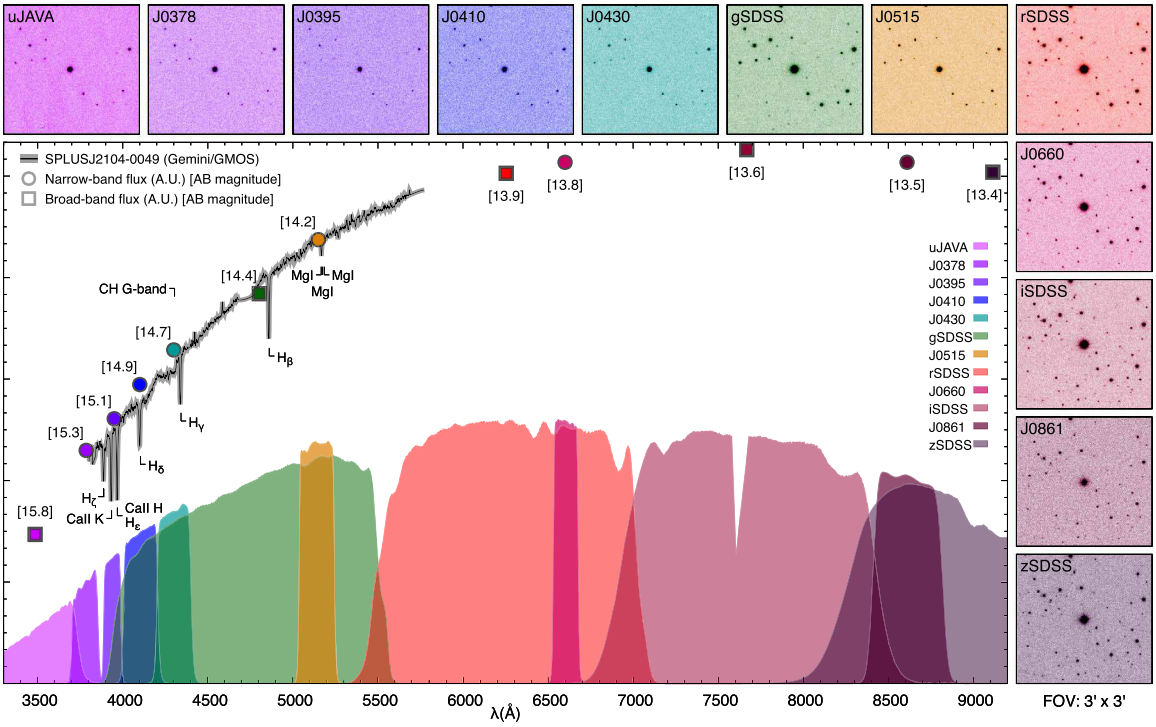

Figure 1. Outside panels: 12-band S-PLUS images for SPLUS J2104−0049, retrieved from the Astro Data Lab. The field of view is $3' \times 3'$, with the north direction up and east to the left. The color of each image is based on the central wavelength of the Javalambre filters, which are named at the top left part of each image. Main panel: transmission curves measured for the set of 12 Javalambre filters, which include the effect of the entire system (sky, mirrors, lenses, and CCD). Also shown are the Gemini/GMOS spectrum (black solid line), the fluxes in the narrowband (filled circles) and broadband (filled squares) filters—calculated from the AB magnitudes (in square brackets). The Gemini/GMOS spectrum is available as the data behind the Figure. The transmission curve data can be obtained from https://github.com/splus-survey/filter_curves.

(The data used to create this figure are available.)

broadness of the *u* filter, which carries most of the metallicity information, the uncertainties increase considerably for [Fe/H] $\leqslant -2.0$.

The *u* and *v* filters from SkyMapper provide extra discriminating power due to their ability to break the degeneracy between surface gravity and metallicity. From its Data Release 1 (DR1; Wolf et al. 2018), photometric atmospheric parameters were determined with a precision better than ∼0.2 dex for [Fe/H] $\geqslant -2.0$ (Casagrande et al. 2019). Another recent effort to search for low-metallicity stars in the Milky Way is the Pristine Survey (Starkenburg et al. 2017), which employs narrowband photometry on the metallicity-sensitive Ca II K absorption feature, in addition to SDSS *g* and *i* filters. The ∼100 Å wide narrowband filter is able to predict metallicities down to [Fe/H] ~ -3.0. A spectroscopic follow-up campaign shows that, out of the 1007 stars observed, ∼70% have [Fe/H] < -2.0 and ∼9% have [Fe/H] < -3.0 (Aguado et al. 2019).

The next generation of narrowband photometric surveys is already underway, building (and improving) upon the successes described above. Two such efforts are the Javalambre Photometric Local Universe Survey (J-PLUS; Cenarro et al. 2019) and the Southern Photometric Local Universe Survey (S-PLUS; Mendes de Oliveira et al. 2019). Both surveys have identical fully robotic telescopes with 0.83 m mirrors and 2.0 deg^2 field of view, performing precision multiple-filter optical photometry (3500–10000 Å) with a set of 12 broadband and narrowband filters, consisting of four SDSS-like (*g*SDSS, *r*SDSS, *i*SDSS, and *z*SDSS), one modified SDSS *u*, and seven narrowband (100–400 Å FWHM) filters. Figure 1 shows the Javalambre photometric system. These filters, by virtue of their restricted bandpasses, have a much higher sensitivity for the determination of stellar atmospheric parameters and selected chemical abundances. In the first attempt to determine metallicities from J-PLUS photometry, Whitten et al. (2019) were able to successfully reproduce spectroscopic values down to [Fe/H] ~ -3.5 with a standard deviation of the residuals $\sigma \sim 0.25$ dex. More recently, Whitten et al. (2021) were able to calculate photometric $T_{\rm eff}$, [Fe/H], and, for the first time, carbon abundances for over 700,000 stars in the S-PLUS DR2 with similar precision.

We report the discovery of SPLUS J210428.01−004934.2 (hereafter SPLUS J2104−0049), a UMP star selected from its narrowband S-PLUS photometry and confirmed by medium- and high-resolution spectroscopy. These proof-of-concept observations are part of an ongoing effort to spectroscopically confirm low-metallicity candidates identified from narrowband photometry.

2. Target Selection and Observations

2.1. Narrowband Photometry

The 12-band photometric data for SPLUS J2104−0049 were obtained during the first S-PLUS observing campaign (Data

Table 1
Observational Data for SPLUS J210428.01−004934.2

Quantity	Symbol	Value	Units	References
R.A.	α (J2000)	21:04:28.01	hh:mm:ss.ss	Gaia Collaboration et al. (2020)
Decl.	δ (J2000)	−00:49:34.2	dd:mm:ss.s	Gaia Collaboration et al. (2020)
Galactic longitude	ℓ	48.7700	degrees	Gaia Collaboration et al. (2020)
Galactic latitude	b	−29.6429	degrees	Gaia Collaboration et al. (2020)
Gaia EDR3 Name		2689845933385992064		Gaia Collaboration et al. (2020)
Parallax	ϖ	0.1619 ± 0.0245	mas	Gaia Collaboration et al. (2020)
Inverse parallax distance	$1/\varpi$	$4.92^{+0.67}_{-0.53}$	kpc	This study[a]
Proper motion (α)	PMRA	14.976 ± 0.027	mas yr^{-1}	Gaia Collaboration et al. (2020)
Proper motion (δ)	PMDec	-8.260 ± 0.017	mas yr^{-1}	Gaia Collaboration et al. (2020)
Mass	M	0.80 ± 0.15	$M_\odot$	Assumed
B magnitude	B	14.978 ± 0.051	mag	Henden & Munari (2014)
V magnitude	V	14.245 ± 0.095	mag	Henden & Munari (2014)
J magnitude	J	12.546 ± 0.023	mag	Skrutskie et al. (2006)
H magnitude	H	12.052 ± 0.024	mag	Skrutskie et al. (2006)
K magnitude	K	11.968 ± 0.028	mag	Skrutskie et al. (2006)
Color excess	$E(B-V)$	0.0557 ± 0.0019	mag	Schlafly & Finkbeiner (2011)
Bolometric correction	BC_V	-0.54 ± 0.08	mag	Casagrande & VandenBerg (2014)
Radial velocity	RV	-110.3 ± 0.5	km s^{-1}	Magellan (MJD: 59166.0389)
Effective Temperature	$T_{\rm eff}$	5045^{+210}_{-95}	K	Gaia Collaboration et al. (2020)
		5044 ± 150	K	This study (Gemini)
		4812 ± 55	K	This study (Magellan)
Log of surface gravity	log g	2.66 ± 0.20	(cgs)	This study (Gemini)
		1.95 ± 0.17	(cgs)	This study (Magellan)
Microturbulent velocity	ξ	1.60 ± 0.20	km s^{-1}	This study (Magellan)
Metallicity	[Fe/H]	-4.22 ± 0.20	dex	This study (Gemini)
		-4.19 ± 0.06	dex	This study LTE (Magellan)
		-4.03 ± 0.10	dex	This study NLTE (Magellan)

Note.
[a] Using $\varpi_{\rm zp} = -0.0414$ mas from Lindegren et al. (2020).

Release 1—DR1[11]) on the Stripe 82, which is a ∼336 deg^2 equatorial field that was first imaged several times by SDSS.

SPLUS J2104−0049 is part of a larger sample of metal-poor star candidates selected based on their position on a color–color diagram constructed using metallicity-sensitive magnitudes, such as J0395 and J0515. Details on the target selection, its effectiveness in identifying chemically peculiar stars, and the spectroscopic follow-up are the subject of a forthcoming paper (V. M. Placco et al. 2021, in preparation). Table 1 summarizes information about SPLUS J2104−0049. Figure 1 shows the 12-band S-PLUS images for SPLUS J2104−0049. Also shown in the main panel are the transmission curves measured for the set of 12 filters, as well as the AB magnitudes (in square brackets).

2.2. Medium-resolution Spectroscopy

The first spectroscopic follow-up of SPLUS J2104−0049 was conducted with the Gemini South Telescope on 2019 May 17, as part of the poor weather program GS-2019A-Q-408. The GMOS-S instrument was used with the B600 l mm^{-1} grating (G5323) and a 1.″0 slit with 2 × 2 binning, resulting in a wavelength coverage in the range [3600:5800] Å at resolving power $R \sim 2000$. The 1200 s exposure resulted in a signal-to-noise ratio (S/N) of S/N ∼ 100 per pixel at the Ca II K line (3933.3 Å). Calibration frames included arc-lamp exposures, bias frames, and quartz flats. All tasks related to spectral reduction, extraction, and wavelength calibration were performed using the Gemini IRAF[12] standard routines.

The central panel of Figure 1 shows the Gemini/GMOS data, scaled in flux by convolving the normalized spectrum with a blackbody curve at $T_{\rm eff} = 4800$ K. Prominent absorption features are identified.

2.3. High-resolution Spectroscopy

The final confirmation step for SPLUS J2104−0049 was the high-resolution spectroscopy, obtained on 2020 November 13 using the MIKE spectrograph mounted on the 6.5 m Magellan-Clay Telescope at Las Campanas Observatory. The observing setup included a 0.″7 slit with 2 × 2 on-chip binning, yielding a resolving power of $R \sim 37{,}000$ ($\lambda < 5000$ Å) and $R \sim 30{,}000$ ($\lambda > 5000$ Å). The S/N is ∼40 per pixel at 3900 Å and ∼120 at 5200 Å after 3200 s of exposure time. The MIKE spectrum covers most of the optical wavelength regime (∼3300–9000 Å), making it suitable for chemical abundance determinations. The blue and red MIKE spectra were reduced using the routines described in Kelson (2003).[13]

3. Stellar Atmospheric Parameters

Stellar atmospheric parameters ($T_{\rm eff}$, log g, and [Fe/H]) were calculated from the Gemini/GMOS spectrum using the n-SSPP (Beers et al. 2014), which is adapted from the SEGUE Stellar

[11] The photometry and images are publicly available at the NSF's NOIRLab Astro Data Lab: https://datalab.noirlab.edu/splus/.

[12] https://www.gemini.edu/observing/phase-iii/understanding-and-processing-data/Data-Processing-Software

[13] http://code.obs.carnegiescience.edu/python

Parameter Pipeline (SSPP; Lee et al. 2008). These parameters were used to select SPLUS J2104−0049 as a candidate for high-resolution spectroscopic follow-up. Table 1 lists $T_{\rm eff}$, log g, and [Fe/H] derived from the Gemini spectrum.

The stellar parameters for the high-resolution data were determined from a combination of photometry, the Gaia parallax (Gaia Collaboration et al. 2020), and the MIKE spectrum. The effective temperature for SPLUS J2104−0049 was calculated from the metallicity-dependent color–$T_{\rm eff}$ relations by Casagrande et al. (2010), adopting [Fe/H] $= -4.0 \pm 0.2$. We used the same procedure outlined in Roederer et al. (2018), drawing 10^5 samples for magnitudes, reddening, and metallicity. The final $T_{\rm eff} = 4812 \pm 55$ K is the weighted mean of the median temperatures for each input color ($B-V$, $V-J$, $V-H$, $V-K$, and $J-K$). The surface gravity was calculated using Equation (1) in Roederer et al. (2018), drawing 10^5 samples from the input parameters listed in Table 1. The final log $g = 1.95 \pm 0.17$ is taken as the median of those calculations with the uncertainty given by their standard deviation.

The equivalent widths were obtained by fitting Gaussian profiles to the observed absorption features. With $T_{\rm eff}$ and log g determined above, the Fe I abundances were determined spectroscopically, using the latest version of the MOOG[14] code (Sneden 1973), employing one-dimensional plane-parallel model atmospheres with no overshooting (Castelli & Kurucz 2004), assuming local thermodynamic equilibrium (LTE). No reliable Fe II features were found in the SPLUS J2104−0049 MIKE spectrum. The microturbulent velocity was determined by minimizing the trend between the abundances of individual Fe I absorption features and their reduced equivalent width. The mean LTE abundance from 51 Fe I lines is [Fe/H] $= -4.19 \pm 0.06$. For 19 of those absorption features, we were able to determine non-LTE (NLTE) abundances using version 1.0 of the `INSPECT`[15] database (Bergemann et al. 2012; Lind et al. 2012). The average difference between the LTE and NLTE abundances is ΔNLTE $= +0.16 \pm 0.03$ and the adopted SPLUS J2104−0049 metallicity for the remainder of this work is [Fe/H] $= -4.03 \pm 0.10$. Table 1 lists the final atmospheric parameters for SPLUS J2104−0049, which will be used for the abundance analysis.

4. Chemical Abundances

Elemental-abundance ratios, [X/Fe], were calculated adopting the solar photospheric abundances from Asplund et al. (2009). The average measurements for 18 elements, derived from the Magellan/MIKE spectrum, are listed in Table 2. The σ values are the standard error of the mean. For σ values below 0.10 dex we set a standard fixed uncertainty of 0.10 dex. For elements with only one detected absorption feature, the uncertainty is determined from the spectral synthesis (see Figure 2). The last column shows which elements had their abundances calculated via equivalent-width analysis (`eqw`) or spectral synthesis (`syn`). The atomic and molecular line lists were generated by the `linemake`[16] code (Placco et al. 2021). Individual references are given in their README file. We have determined NLTE abundance corrections for three elements besides Fe I: Al I, Cr I, and Mn I. The values and references are given in Table 2.

Table 2
Abundances for Individual Species

Ion	log $\epsilon_\odot$ (X)	log ϵ (X)	[X/H]	[X/Fe]	σ	N	
Li I	1.05	0.41	⋯	⋯	0.15	1	syn
C	8.43	4.34	−4.09	−0.06	0.15	3	syn
Na I	6.24	1.98	−4.26	−0.23	0.10	2	eqw
Mg I	7.60	3.94	−3.66	+0.37	0.10	4	eqw
Al I[a]	6.45	2.37	−4.08	−0.05	0.15	2	syn
Si I	7.51	4.07	−3.44	+0.59	0.15	1	syn
Ca I	6.34	2.63	−3.71	+0.32	0.10	2	syn
Sc II	3.15	−0.65	−3.80	+0.23	0.10	5	eqw
Ti II	4.95	1.22	−3.73	+0.30	0.10	9	eqw
V II	3.93	0.39	−3.54	+0.49	0.20	1	syn
Cr I[b]	5.64	1.35	−4.29	−0.26	0.10	2	eqw
Mn I[c]	5.43	0.75	−4.68	−0.65	0.10	2	syn
Fe I[d]	7.50	3.47	−4.03	0.00	0.10	19	eqw
Co I	4.99	1.15	−3.84	+0.19	0.10	3	eqw
Ni I	6.22	2.22	−4.00	+0.03	0.10	3	eqw
Zn I	4.56	1.17	−3.39	+0.64	0.20	1	syn
Sr II	2.87	−2.07	−4.94	−0.91	0.15	2	syn
Ba II	2.18	−3.06	−5.24	−1.21	0.20	2	syn

Notes.
[a] ΔNLTE $= +0.60$ (Nordlander & Lind 2017).
[b] ΔNLTE $= +0.35$ (based on the empirical corrections of Roederer et al. 2014b).
[c] ΔNLTE $= +0.60$ (Bergemann & Gehren 2008).
[d] ΔNLTE $= +0.16$ (Bergemann et al. 2012; Lind et al. 2012).

Overall, SPLUS J2104−0049 has the chemical abundance pattern of a "typical" UMP star (apart from carbon—see discussion in Section 5). The lithium abundance is consistent with its evolutionary stage and the light-element abundance ratios [X/Fe] (from Na to Zn) are in agreement with general trends found in the literature at this metallicity regime (Abohalima & Frebel 2018). The same applies to the low abundance ratios found for the heavy elements Sr and Ba. The upper panel of Figure 2 shows the spectral synthesis of the CH G-band at λ4304 Å for SPLUS J2104−0049. The lower panels show the same procedure for the Li I λ6707 Å and Sr II λ4077 Å absorption features. Even though SPLUS J2104−0049 is on the red giant branch, there is no carbon depletion due to CN processing, which is a result of the combination of its low metallicity and low carbon abundance (see Figure 9 in Placco et al. 2014).

5. Possible Origins for SPLUS J2104−0049

The current working hypothesis in stellar archeology is that UMP stars are bona fide second-generation objects chemically enriched by a single Population III supernova ("mono-enriched"); thus their chemical abundance pattern is a direct result of the composition of the parent gas cloud. Below we present possible formation pathways and stellar progenitors that could account for the existence of SPLUS J2104−0049 and its low carbon content.

SPLUS J2104−0049 is the 35th UMP star identified to date (Suda et al. 2008; Abohalima & Frebel 2018).[17] Among these, only three *are not* classified as carbon-enhanced metal-poor (CEMP; [C/Fe] $\geqslant +0.7$, Aoki et al. 2007): CD−38°245 (Spite

[14] https://github.com/alexji/moog17scat
[15] http://www.inspect-stars.com/
[16] https://github.com/vmplacco/linemake
[17] The SAGA database was last updated on 2020 November 9.

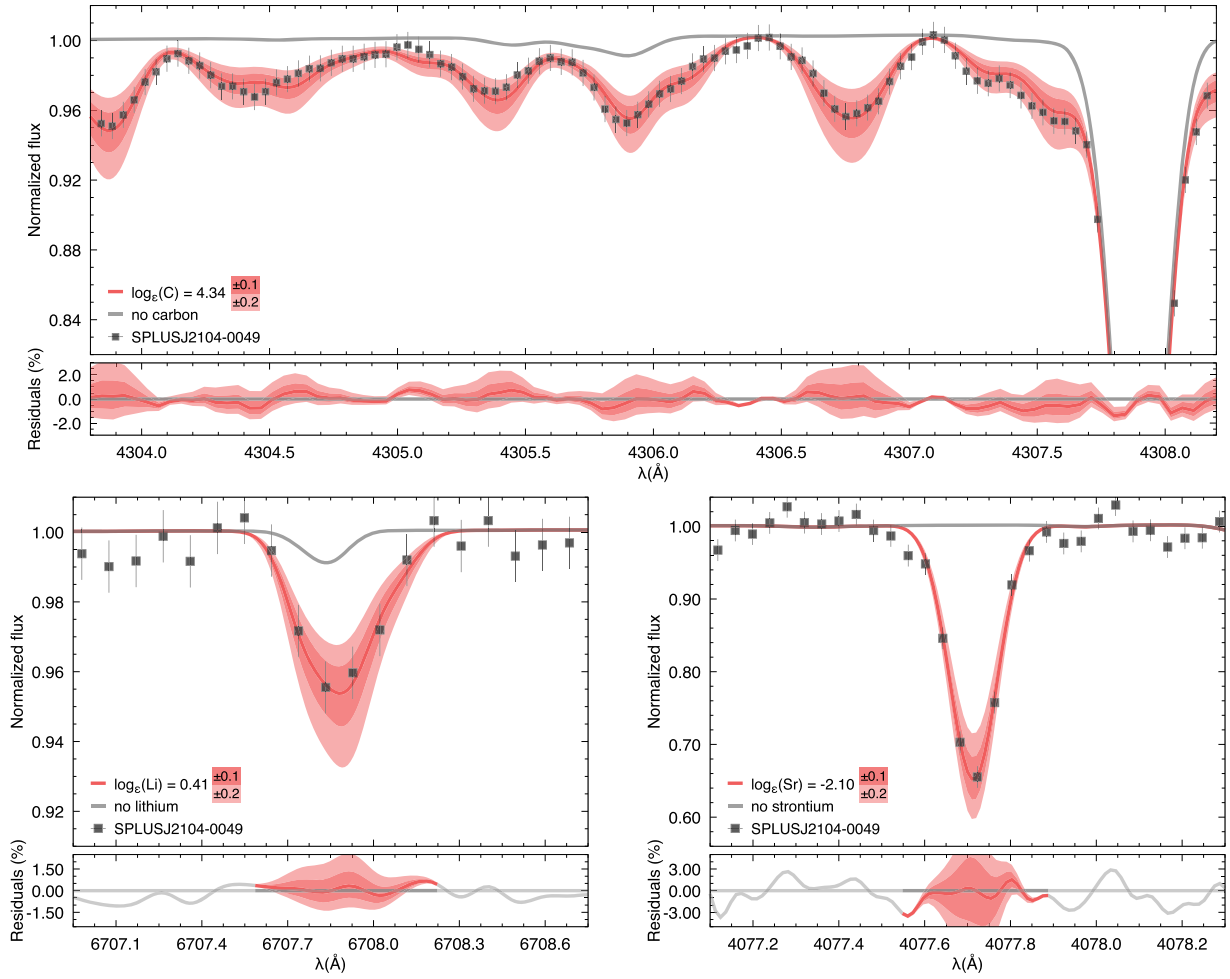

Figure 2. Spectral syntheses for the determination of carbon (upper panel), lithium (lower left panel), and strontium (lower right panel) abundances. The top panel of each plot shows the best-fit syntheses (red lines) and uncertainties (±0.1 and ±0.2 dex—shaded regions) compared to the observed spectra (points). Also shown are syntheses after removing the contributions from specific elements (gray lines).The bottom panels show the percent residuals between the observed spectra and the syntheses.

et al. 2005, [C/Fe] < -0.33), CS 22963−004 (Lai et al. 2008, [C/Fe] $= +0.40$), and now SPLUS J2104−0049 ([C/Fe] $= -0.06$), with the lowest A(C)[18] value ever *detected* in the [Fe/H] < -4.0 regime. The upper panel of Figure 3 shows the $A(\mathrm{C})_{\mathrm{cor}}$[19] versus [Fe/H] distribution for stars in the literature with [Fe/H] < -2.5 (blue filled squares) compared to SPLUS J2104−0049 (red filled circle). Also shown are stripe-density profiles and the line defining the CEMP criteria. Based on these data (and with the addition of SPLUS J2104 −0049), the CEMP fraction among UMP stars is 91^{+6}_{-14} %[20] (32/35—including A(C) upper limits) and 92^{+6}_{-17}% (23/25—excluding upper limits). These are larger, nonetheless consistent, with the 81% fraction calculated by Placco et al. (2014).

The low carbon abundance in SPLUS J2104−0049 helps constrain the main cooling channel that allowed its parent gas cloud to fragment. According to Chiaki et al. (2017), there is insufficient cooling from carbon dust grains for $A(\mathrm{C}) \lesssim 5.8$, so the most efficient way to induce cloud fragmentation would be by silicate dust cooling. In fact, SPLUS J2104−0049 resides in the "silicate dominant" regime in the A(C)-[Fe/H] diagram (see Figure 2 of Chiaki et al. 2017). An additional diagnostic to assess whether a star is "mono-enriched" is through its [Mg/C] abundance ratio (Hartwig et al. 2018). The low metallicity of SPLUS J2104−0049, coupled with its [Mg/C] $= +0.43$, places it well within the realm of the simulated mono-enriched second-generation stars by Hartwig et al. (2018).

From the hypothesis that SPLUS J2104−0049 is a second-generation star,[21] it is possible to further investigate the characteristics of its massive stellar parent. For this, we have used the set of theoretical nucleosynthesis yields (`znuc2012.S4`) from Heger & Woosley (2010),[22] which model the explosion of 16,800 metal-free stars with masses from 10 to 100 $M_\odot$ and explosion energies from 0.3×10^{51} erg to 10×10^{51} erg. To compare the chemical abundance pattern of SPLUS J2104−0049 with the theoretical values, we followed the same procedure first described in Roederer et al. (2016), generating 10^4 sets of abundances by resampling the $\log \epsilon$(X) and σ values from Table 2, assuming Gaussian distributions.

[18] $A(\mathrm{C}) = \log(N_\mathrm{C}/N_\mathrm{H}) + 12$.

[19] The observed A(C) values have been corrected following the prescriptions found in Placco et al. (2014).

[20] Uncertainties in the fractions are the Wilson score confidence intervals.

[21] If the assumption that SPLUS J2104−0049 is a second-generation star is valid, then the presence of the heavy elements Sr and Ba in its atmosphere indicate that at least one neutron-capture event must be accounted for in some of the first stars (Roederer et al. 2014a; Banerjee et al. 2018).

[22] http://starfit.org

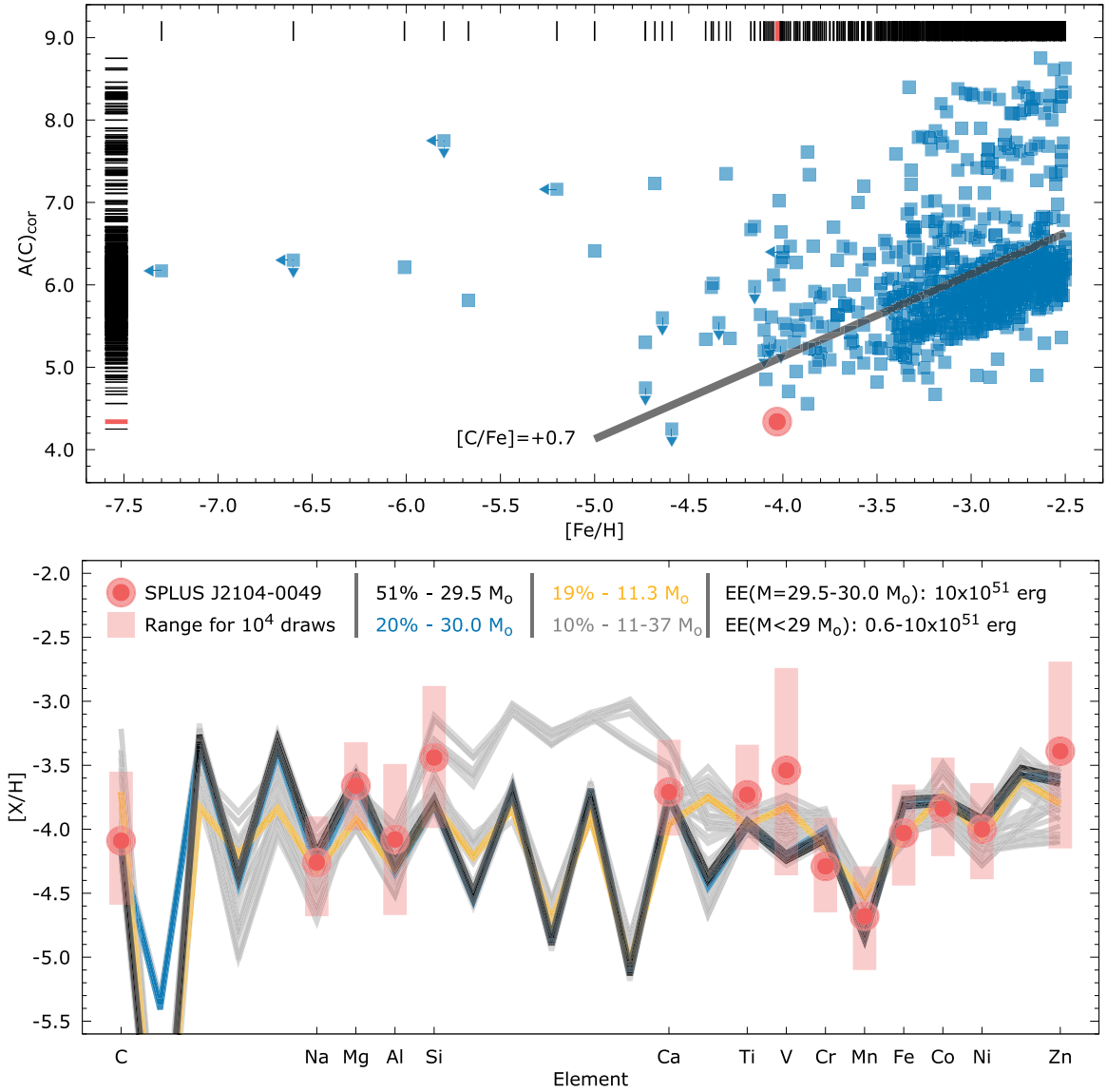

Figure 3. Upper panel: carbon abundances—A(C)—as a function of the metallicity–[Fe/H]—for SPLUS J2104−0049 (filled circle) and the literature compilations JINAbase (Abohalima & Frebel 2018) and SAGA (Suda et al. 2008) (filled squares). The solid line represents the current criteria for CEMP stars ([C/Fe] = +0.7). Upper limits are only shown for [Fe/H] ⩽ −4.0. Stripe-density profiles are also shown, with the values for SPLUS J2104−0049 highlighted. The upper panel is also available as a Bokeh-generated interactive figure. Hovering the mouse over any point will reveal the underlying data including the name, atmospheric parameters, carbon abundances, upper limit flags, and source. Other functionalities are available via the buttons at the top of the interactive figure. Hovering the mouse over each will reveal its functionality, i.e., panning, zooming, reset. The underlying data set is also available in machine-readable format via the figure data file link. A bigger version that will be updated as more data become available is available at http://vmplacco.github.io/files/acfeh.html. Lower panel: best model fits for SPLUS J2104 −0049. The solid lines show the theoretical predictions from the Heger & Woosley (2010) `znuc2012.S4` models, color coded by mass and occurrence fraction within the 10^4 simulations. The explosion energies (EEs) are also listed. The solid circles are the measured abundances for SPLUS J2104−0049, and the shaded areas mark the range of simulated abundances.

The results of this exercise, shown in the lower panel of Figure 3 strongly imply (∼71% of the simulations) a suitable stellar progenitor for SPLUS J2104−0049 in the 29.5–30.0 $M_\odot$ range with an explosion energy of 10×10^{51} erg. In particular, the 29.5 $M_\odot$ model (black solid line) is able to reproduce the low [C/H] of SPLUS J2104−0049 while still providing reasonably good fits for the other elements. Even though the 11.3 $M_\odot$ model provides the best fit in 19% of the simulations, its carbon abundance is consistently higher than the SPLUS J2104−0049 detection. The range of masses found for the progenitors of carbon-enhanced UMP stars in Placco et al. (2016), 29.5–30.0 $M_\odot$, is similar to the ones found here for a much lower carbon abundance. However, the explosion energies found for the Placco et al. (2016) sample are lower by a factor of ∼15–30, suggesting that this may be one of the drivers for the distinct chemical signatures found in UMP stars. It is also worth noting that the best-fit models tend to produce lower amounts of silicon when compared to SPLUS J2104 −0049, in contrast to the lower-energy models that better reproduce the observed Si abundance. This reinforces the need for observing additional UMP stars, in particular with low carbon abundances.

6. Conclusions and Future Work

We have presented the first spectroscopic follow-up study of the UMP star SPLUS J2104−0049. This star was first identified from its narrowband S-PLUS photometry. High-

resolution spectroscopy revealed a unique chemical abundance pattern, with the lowest carbon abundance ever measured for a UMP star. Comparison with theoretical models suggest that SPLUS J2104−0049 is a second-generation star formed in a gas cloud polluted by the byproducts of the evolution of a progenitor in the $\sim 30\,M_{\odot}$ range with an explosion energy of 10×10^{51} erg. Additional UMP stars identified from S-PLUS photometry will greatly improve our understanding of Population III stars and enable the possibility of finding a metal-free low-mass star still living in our Galaxy today.

The authors would like to thank the anonymous referee and the members of the S-PLUS community who provided insightful comments on the manuscript. The work of V.M.P. is supported by NOIRLab, which is managed by the Association of Universities for Research in Astronomy (AURA) under a cooperative agreement with the National Science Foundation. I.U.R. acknowledges financial support from grants AST 16-13536, AST-1815403, and PHY 14-30152 (Physics Frontier Center/JINA-CEE) awarded by the NSF. Y. S.L. acknowledges support from the National Research Foundation (NRF) of Korea grant funded by the Ministry of Science and ICT (NRF-2018R1A2B6003961 and NRF-2021R1A2C1008679). F.R.H. thanks FAPESP for the financial support through the grant 2018/21661-9. H.D.P. thanks FAPESP for the financial support through the grant 2018/21250-9. The S-PLUS project, including the T80-South robotic telescope and the S-PLUS scientific survey, was founded as a partnership between the Fundação de Amparo à Pesquisa do Estado de São Paulo (FAPESP), the Observatório Nacional (ON), the Federal University of Sergipe (UFS), and the Federal University of Santa Catarina (UFSC), with important financial and practical contributions from other collaborating institutes in Brazil, Chile (Universidad de La Serena), and Spain (Centro de Estudios de Física del Cosmos de Aragón, CEFCA). We further acknowledge financial support from the São Paulo Research Foundation (FAPESP), the Brazilian National Research Council (CNPq), the Coordination for the Improvement of Higher Education Personnel (CAPES), the Carlos Chagas Filho Rio de Janeiro State Research Foundation (FAPERJ), and the Brazilian Innovation Agency (FINEP). The members of the S-PLUS collaboration are grateful for the contributions from CTIO staff in helping in the construction, commissioning and maintenance of the T80-South telescope and camera. We are also indebted to Rene Laporte, INPE, and Keith Taylor for their important contributions to the project. From CEFCA, we thank Antonio Marín-Franch for his invaluable contributions in the early phases of the project, David Cristóbal-Hornillos and his team for their help with the installation of the data reduction package JYPE version 0.9.9, César Íñiguez for providing 2D measurements of the filter transmissions, and all other staff members for their support with various aspects of the project. This research uses services or data provided by the Astro Data Lab at NSF's NOIRLab. NOIRLab is operated by the Association of Universities for Research in Astronomy (AURA), Inc. under a cooperative agreement with the National Science Foundation. This research was made possible through the use of the AAVSO Photometric All-Sky Survey (APASS), funded by the Robert Martin Ayers Sciences Fund. This work has made use of data from the European Space Agency (ESA) mission Gaia (https://www.cosmos.esa.int/gaia), processed by the Gaia Data Processing and Analysis Consortium (DPAC, https://www.cosmos.esa.int/web/gaia/dpac/consortium). Funding for the DPAC has been provided by national institutions, in particular the institutions participating in the Gaia Multilateral Agreement.

Software: `awk` (Aho et al. 1987), `bokeh` (Bokeh Development Team 2018), `CarPy` (Kelson 2003), `gnuplot` (Williams & Kelley 2015), `IRAF` (Tody 1986, 1993), `linemake` (Placco et al. 2021), `MOOG` (Sneden 1973), `n-SSPP` (Beers et al. 2014, 2017), `sed` (Mcmahon 1979).

ORCID iDs

Vinicius M. Placco https://orcid.org/0000-0003-4479-1265
Ian U. Roederer https://orcid.org/0000-0001-5107-8930
Young Sun Lee https://orcid.org/0000-0001-5297-4518
Fábio R. Herpich https://orcid.org/0000-0001-7907-7884
Hélio D. Perottoni https://orcid.org/0000-0002-0537-4146
William Schoenell https://orcid.org/0000-0002-4064-7234
Tiago Ribeiro https://orcid.org/0000-0002-0138-1365

References

Abohalima, A., & Frebel, A. 2018, ApJS, 238, 36
Aguado, D. S., Youakim, K., González Hernández, J. I., et al. 2019, MNRAS, 490, 2241
Aho, A. V., Kernighan, B. W., & Weinberger, P. J. 1987, The AWK Programming Language (Boston, MA: Addison-Wesley Longman Publishing Co., Inc.)
Aoki, W., Beers, T. C., Christlieb, N., et al. 2007, ApJ, 655, 492
Asplund, M., Grevesse, N., Sauval, A. J., & Scott, P. 2009, ARA&A, 47, 481
Banerjee, P., Qian, Y.-Z., & Heger, A. 2018, ApJ, 865, 120
Beers, T. C., & Christlieb, N. 2005, ARA&A, 43, 531
Beers, T. C., Norris, J. E., Placco, V. M., et al. 2014, ApJ, 794, 58
Beers, T. C., Placco, V. M., Carollo, D., et al. 2017, ApJ, 835, 81
Bergemann, M., & Gehren, T. 2008, A&A, 492, 823
Bergemann, M., Lind, K., Collet, R., Magic, Z., & Asplund, M. 2012, MNRAS, 427, 27
Bokeh Development Team 2018, Bokeh: Python Library for Interactive Visualization, https://bokeh.pydata.org/en/latest/
Bromm, V. 2013, RPPh, 76, 112901
Casagrande, L., Ramírez, I., Meléndez, J., Bessell, M., & Asplund, M. 2010, A&A, 512, A54
Casagrande, L., & VandenBerg, D. A. 2014, MNRAS, 444, 392
Casagrande, L., Wolf, C., Mackey, A. D., et al. 2019, MNRAS, 482, 2770
Castelli, F., & Kurucz, R. L. 2004, in IAU Symp. 210, Modelling of Stellar Atmospheres, ed. N Piskunov (San Francisco, CA: ASP), A20
Cenarro, A. J., Moles, M., Cristóbal-Hornillos, D., et al. 2019, A&A, 622, A176
Chiaki, G., Tominaga, N., & Nozawa, T. 2017, MNRAS, 472, L115
Dopcke, G., Glover, S. C. O., Clark, P. C., & Klessen, R. S. 2013, ApJ, 766, 103
Gaia Collaboration, Brown, A. G. A., Vallenari, A., et al. 2020, arXiv:2012.01533
Hartwig, T., Bromm, V., Klessen, R. S., & Glover, S. C. O. 2015, MNRAS, 447, 3892
Hartwig, T., Yoshida, N., Magg, M., et al. 2018, MNRAS, 478, 1795
Heger, A., & Woosley, S. E. 2010, ApJ, 724, 341
Henden, A., & Munari, U. 2014, CoSka, 43, 518
Keller, S. C., Bessell, M. S., Frebel, A., et al. 2014, Natur, 506, 463
Kelson, D. D. 2003, PASP, 115, 688
Lai, D. K., Bolte, M., Johnson, J. A., et al. 2008, ApJ, 681, 1524
Lee, Y. S., Beers, T. C., Sivarani, T., et al. 2008, AJ, 136, 2022
Lind, K., Bergemann, M., & Asplund, M. 2012, MNRAS, 427, 50
Lindegren, L., Bastian, U., Biermann, M., et al. 2020, arXiv:2012.01742
Mcmahon, L. E. 1979, UNIX Programmer's Manual—7th ed., Vol. 2 (Murray Hill: Bell Telephone Laboratories)
Mendes de Oliveira, C., Ribeiro, T., Schoenell, W., et al. 2019, MNRAS, 489, 241
Nordlander, T., & Lind, K. 2017, A&A, 607, A75
Placco, V. M., Frebel, A., Beers, T. C., et al. 2016, ApJ, 833, 21
Placco, V. M., Frebel, A., Beers, T. C., & Stancliffe, R. J. 2014, ApJ, 797, 21
Placco, V. M., Sneden, C., Roederer, I., et al. 2021, RNAAS, 5, 92

Roederer, I. U., Placco, V. M., & Beers, T. C. 2016, ApJL, 824, L19
Roederer, I. U., Preston, G. W., Thompson, I. B., Shectman, S. A., & Sneden, C. 2014a, ApJ, 784, 158
Roederer, I. U., Preston, G. W., Thompson, I. B., et al. 2014b, AJ, 147, 136
Roederer, I. U., Sakari, C. M., Placco, V. M., et al. 2018, ApJ, 865, 129
Schlafly, E. F., & Finkbeiner, D. P. 2011, ApJ, 737, 103
Schlaufman, K. C., Thompson, I. B., & Casey, A. R. 2018, ApJ, 867, 98
Ivezić, Ž., Sesar, B., Jurić, M., et al. 2008, ApJ, 684, 287
Skrutskie, M. F., Cutri, R. M., Stiening, R., et al. 2006, AJ, 131, 1163
Sneden, C. A. 1973, PhD thesis, The University of Texas at Austin
Spite, M., Cayrel, R., Plez, B., et al. 2005, A&A, 430, 655
Stacy, A., Bromm, V., & Lee, A. T. 2016, MNRAS, 462, 1307
Starkenburg, E., Martin, N., Youakim, K., et al. 2017, MNRAS, 471, 2587
Suda, T., Katsuta, Y., Yamada, S., et al. 2008, PASJ, 60, 1159
Tody, D. 1986, Proc. SPIE, 627, 733
Tody, D. 1993, in ASP Conf. Ser. 52, Astronomical Data Analysis Software and Systems II, ed. R. J. Hanisch, R. J. V. Brissenden, & J. Barnes (San Francisco, CA: ASP), 173
Whitten, D. D., Placco, V. M., Beers, T. C., et al. 2019, A&A, 622, A182
Whitten, D. D., Placco, V. M., Beers, T. C., et al. 2021, arXiv:2104.00016
Williams, T., & Kelley, C. 2015, Gnuplot 5.0: An Interactive Plotting Program, http://www.gnuplot.info/
Wolf, C., Onken, C. A., Luvaul, L. C., et al. 2018, PASA, 35, e010
York, D. G., Adelman, J., Anderson, J. E., Jr., et al. 2000, AJ, 120, 1579